PAPER REF: 3932

# COATINGS SUPPORTED ON FECRALLOY: LINKS BETWEEN SURFACE TREATMENT, PARTICLE SIZE & COATING PROPERTIES

**Stephen Adegbite**[1(*)]

[1]Engineering and Physical Sciences, University of Birmingham, Edgbaston, Birmingham, B15 2TT, UK
(*)*Email:* s.adegbite@surrey.ac.uk; stephen_adegbite@hotmail.com

## ABSTRACT

Tightening legislation for vehicles across the world has caused the use of monolith catalysts in automotive emission control catalysts to become prevalent. Therefore it is of upmost importance to ensure good adhesion of the active phase coating onto the monolith surface to maximise performance. An automatic film applicator is used for coating γ–alumina slurries onto Fecralloy, an integral component of metallic monolith catalysts. Fecralloy coupons pre-oxidised at 950$^{o}$C for 10 h were found to give the best adhesion in terms of coating loading (~8 mass %) and adhesion (< 10 mass % loss). These conditions produced the optimal surface topography, typified by conspicuous and randomly-oriented α–alumina whiskers which promote coating adhesion. The finest particle coatings of 40 wt% solids concentration produced the best adhesion because their maximum particle size was not larger than the asperities on the surface of the Fecralloy.

***Keywords:*** γ–alumina, coating, adhesion, pre-oxidation, Fecralloy, mechanical.

## 1. INTRODUCTION

From 1940 to 1950s air quality problems were experienced in some urban cities in the USA because of the increasing numbers of cars (Haagen-Smit et al., 1953). The first major applications of monolith catalysts (Fig. 1) during this period were for automotive emission control and for the decolourisation of nitric acid tail gas.

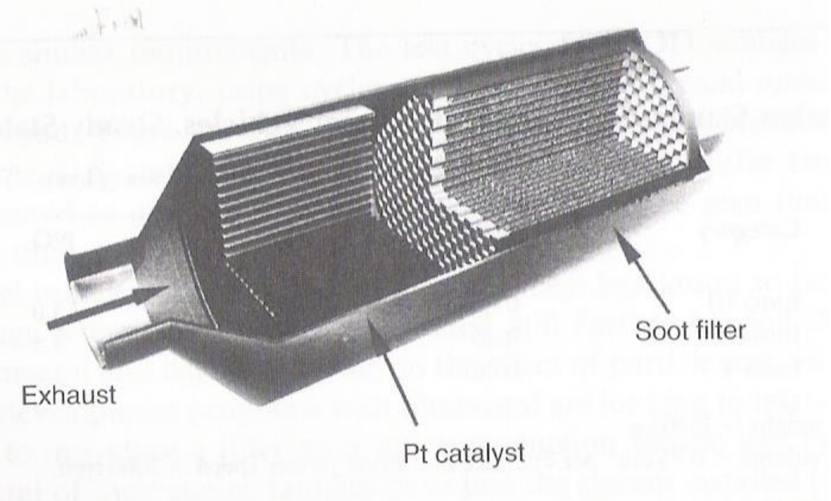

Fig. 1. Schematic diagram of the motor vehicle catalyst used for emission control (Cybulski and Moulijn, 2006).

In the late 1960s researchers in the USA began to develop more interests in monoliths in their quest for effective afterburner catalysts because of their characteristic low pressure drop. This led to the development and industrial production of monolith catalysts of increased longevity which would meet the requirements of the 1970 Clean Air Act (Nievergeld, 1998; Cybulski and Moulijn, 1994). The emergence of the first cars equipped with monolith catalysts began in 1975. Today there are several hundred millions of monolith catalysts fitted in motor vehicles worldwide (Twigg, 2007). The exhaust gas stream consists of 3 major pollutants: carbon monoxide (CO), oxides of nitrogen (NO) and hydrocarbons (HCs). This stream is converted inside the exhaust pipe, which houses the catalyst, into environmentally less harmful products (such as nitrogen gas and carbon dioxide).

Throughout the last three decades the advancements in emission control technology have been propelled by stringent legislation (Fig. 2). One major success worth noting is that since 1975 emission levels from exhaust systems of passenger cars have fallen by more than 90% (relative to the 1960s), with future targets aimed at zero emissions (Twigg, 2006; Acres and Harrison, 2004).

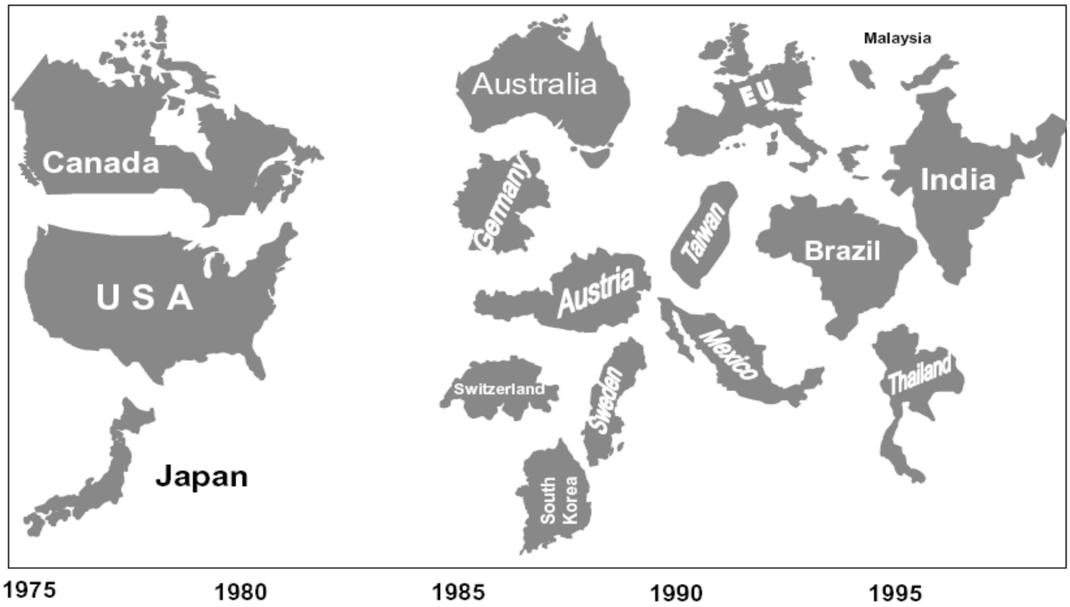

Fig. 2. Introduction of emission control legislation across the world (Acres and Harrison, 2004).

Europe originally lagged behind the USA with automotive catalyst fitting not required until 1993, and is now catching up according to the recent trends in legislation (Collins and Twigg, 2007). Today all countries in the world that legislate for emissions have adopted either the USA (i.e. Federal Test Procedure) or the European (i.e. Motor Vehicle Emissions Group) regulation test except for Japan, which has its own test. For instance, China and India use the European test, while South America uses the USA test (Cybulski and Moulijn, 2006).

Monolith catalysts are manufactured in industry by coating γ–alumina slurries – the carrier of the platinum group metals (PGMs) – onto structured catalyst supports. Monoliths are honeycomb materials (Fig. 3) that act as catalyst supports (i.e. substrates) upon which coating slurries are deposited. They have channels which are straight and parallel. They are of two types: metallic monoliths, made from Fecralloy; and ceramic monoliths, mostly made from cordierite (Avila et al., 2005).

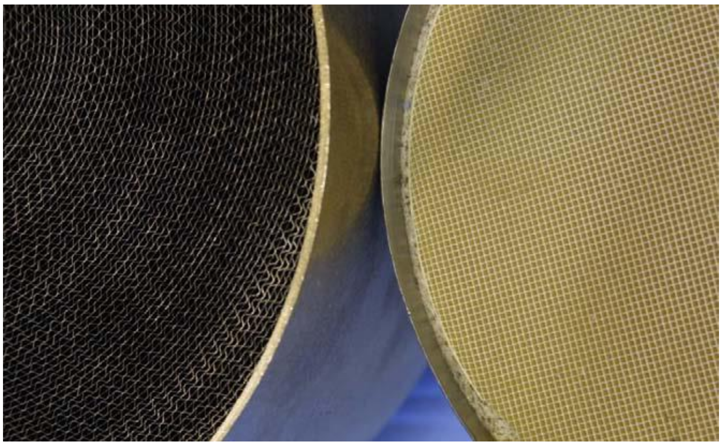

Fig. 3. Examples of metal-based catalyst (left) and ceramic-based cordierite catalyst (right) (Twigg, 2006).

Manufacture of the monolith catalysts presents several challenges, the greatest of which is obtaining sufficient adhesion between the platinum group metal (PGM) inorganic slurry and the monolith support to prevent flaking or defects forming in the surface coating over the operating life of the component (Twigg, 2006). Metal monoliths have significantly thinner walls compared to ceramic monoliths, and this enables the former to have a much shortened warm-up period which leads to increased catalytic efficiency (Sun et al., 2007; Fei et al., 2003). On the other hand, ceramic monoliths are relatively cheap and have large pores which absorb the slurry, and this improves the coating adhesion. The thermal expansion of the coating is also similar to ceramic monoliths compared to metal (Williams, 2001). These problems can however be tackled by proper slurry formulation, and the use of metal monoliths which are based on an appropriate alloy, such as Fecralloy®, that is specially processed to form an adherent and stable alumina surface layer (Jia et al., 2007; Cybulski and Moulijn, 2006; Burgos et al., 2003). The quality of monolith catalysts is determined by their performance-determining properties, such as loading, adherence, thickness and homogeneity. In addition to this, when the rheology and the particle size distributions (psds) of the coating slurry are not properly optimised, the end result can be poor coating adhesion, which results in the untimely loss of PGMs and catalytic inefficiency (Agrafiotis et al., 2000).

A preparation path for coatings (Fig. 4) shows the critical factors at each process unit which can influence the coating quality. The $\gamma$–alumina particles contained in the slurry are milled to a desired particle size distribution at a controlled pH to prevent aggregation. The slurry is then deposited onto the monolith, pre-oxidised in a furnace between 900 and 1200 $^{o}$C for 5 – 30 h, to generate a substrate/ washcoat composite, which is subsequently dried and calcined (Jia et. al, 2007). A literature survey has shown that the main used method of coating Fecralloy® in the laboratory is by dip-coating (Jia et al., 2007; Zhao et al., 2003; Fei et al., 2003; Valentini et al., 2001), though other methods have been used, such as electrophoretic deposition (Sun et al., 2007), chemical vapour deposition (Janickle et al., 2000), physical vapour deposition (Kestenbaum et al., 2002). The common disadvantage of dip-coating is the inconsistency in the coating quality as evidenced from the wide variation in the coating loadings (Jia et al., 2007) and the difficulty in controlling the shear rates at which the slurry is coated. The assessment of coating adhesion in previous studies has empirically been based on the mass loss from ultrasonic vibration (Zhao et al., 2003; Valentini et al., 2001), while few studies have also used thermal shock (Jia et al., 2007), drop test (Germani et al., 2007) and scratch test (Roth et al, 1987). The ultrasonic vibration test involves the soaking of coatings in petroleum ether, and then treating them in an ultrasonic vibrator for 5 – 60 min. The petroleum ether, being a non-polar solvent which contains mostly pentane, acts by weakening the attractive bonds in the coatings (Housecroft and Constable, 2002). The treated sample is dried afterwards and the mass loss is evaluated. None of these methods provides a measure of the coating failure strength or whether the coatings fail in adhesion (between the coatings and the surface) or in cohesion (within the coatings itself). Therefore, existing tests only provide relative data which can be linked to the performance of the component.

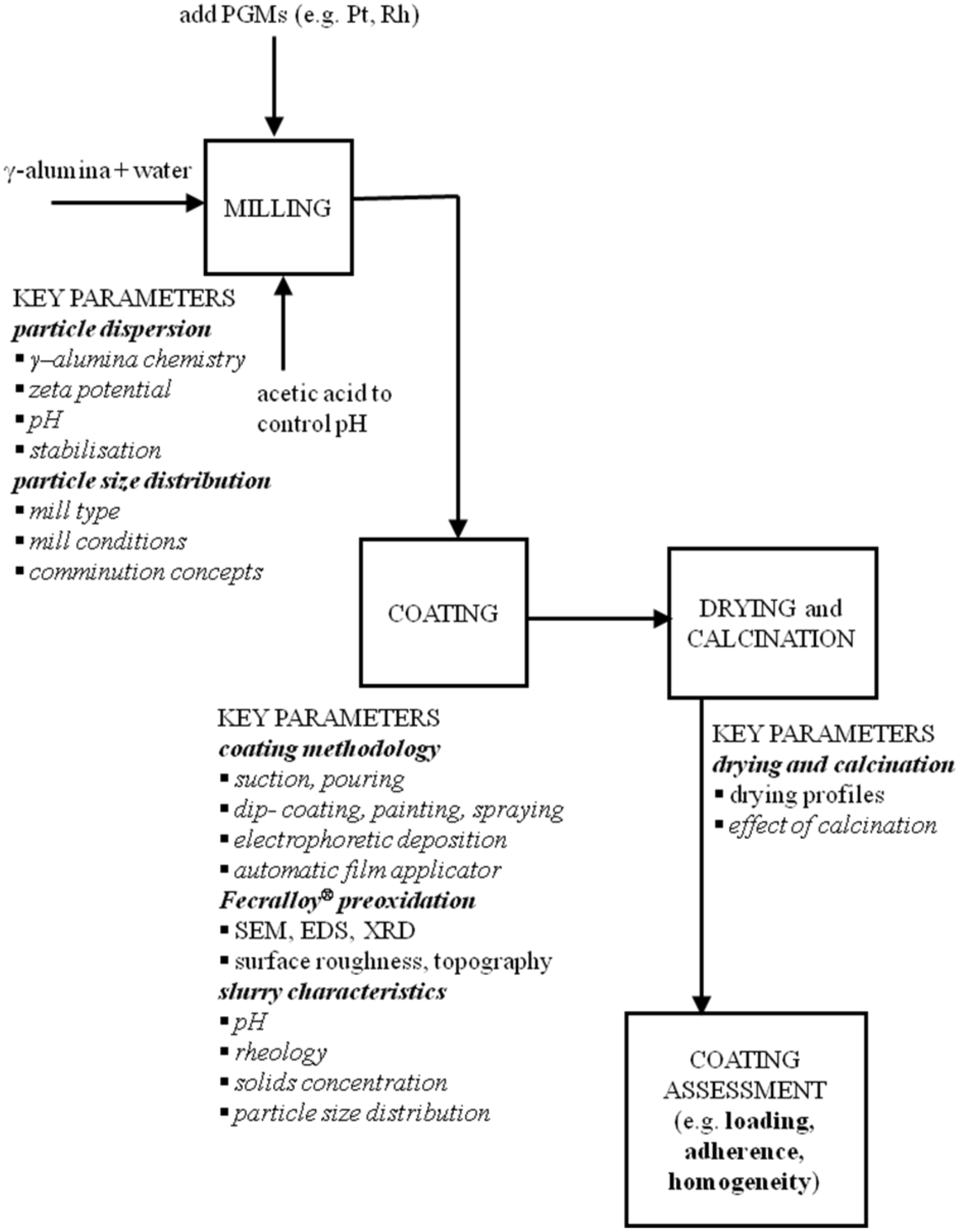

Fig. 4. A preparation path for coatings.

In this paper, the X-ray diffraction (XRD) and scanning electron microscope (SEM) equipped with an energy-dispersive spectrometer (EDS) are used to assess the influence of pre-oxidation treatment on the Fecralloy efficacy as a catalyst support. The surface topography of Fecralloy has been measured using laser profiling interferometry (LPI). Categories of γ–alumina slurries with varying particle size distribution ($d_{0.9}$ = 7.8 – 33.4μm) and solids concentration (15 – 45 wt%) have been coated onto pre-oxidised Fecralloy coupons using an automatic film applicator enabling control of the coating process conditions, such as applied shear rate. Upon drying and calcination at 110 $^{o}$C and 500 $^{o}$C respectively, the coating adhesion has been measured using ultrasonic vibration and a new mechanical testing method, which is physically derived test that measures the profile of the coating failure strength. The conditions for optimal coating adhesion are obtained from the experimental data.

## 2. MATERIALS AND METHODS

### *2.1. Slurry preparation and characterisation*

The γ–alumina powder (PURALOX SCFa-140, Sasol UK) has a specific surface area of 142 $m^2g^{-1}$ and 90 percentile diameter $d_{0.9}$ of 43.4 μm. The slurries were prepared by adding γ–alumina powder in doubly distilled water, with the pH adjusted to a value of 4 using acetic acid solution (1M; Fischer Scientific, UK). As the slurry pH can affect the adhesion of γ–alumina coatings onto Fecralloy®, the previous studies (e.g. Adegbite, 2010; Jia et al., 2007) have shown that at pH of 4 – 6 the γ–alumina particles are well dispersed and far away from the isoelectric point, therefore enabling optimal coating adhesion. The slurry particles were then mixed and comminuted inside a stirred bead mill of volume = 1.2 litre (Union Process, USA). Spherical zirconia grinding media of 5 mm diameter were added at 40 vol.% and the milling time was set to either 10, 20, 40, 60 or 240 min at a rotating shaft speed of 500 rpm. The milling temperature was kept between 20 – 22 $^{o}$C via a cooling jacket.

A laser diffraction equipment (Mastersizer 2000, Malvern Instruments UK) was used for measuring the particlesize distributions (psds) of the slurries. The volume particle size distributions (Fig. 5) show that the unmilled slurry has a unimodal distribution having a peak at 30 μm, with a shoulder and a long tail towards the smallest particle sizes (1- 10 μm). As the milling time increases, the peak shifts towards smaller sizes due to the comminution of the particles. The diameter $d_{0.9}$ measurements reduce from 43.4 μm for the unmilled sample to 7.8 μm for the sample milled for 240 min (Table 1). The steady shear rheology of the slurries was measured using a stress-controlled AR 1000 rheometer (TA Instruments, UK) equipped with a 40mm parallel plate geometry and roughened to eliminate wall slip.

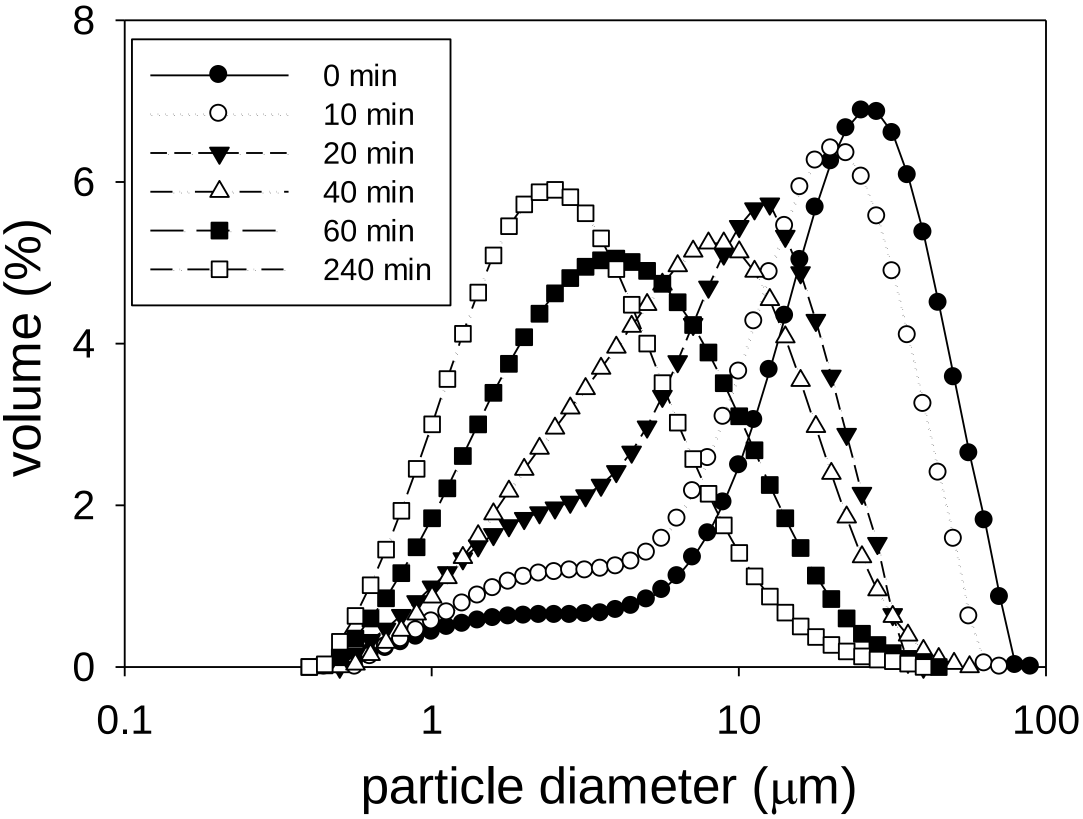

Fig. 5. Particle size distributions of slurries of 40 wt% solids concentration after milling for 0 – 240 min.

Table 1. Properties of milled slurries: particle size distribution.

| Slurry | Milling time $t_m$ (min) | 10% diameter $d_{0.1}$ (μm) | 50% diameter $d_{0.5}$ (μm) | 90% diameter $d_{0.9}$ (μm) | Consistency index K (Pas$^n$) | Power law exponent n (-) |
|---|---|---|---|---|---|---|
| $S_0$ | 0 | 4.6 | 20.7 | 43.4 | - | - |
| $S_{10}$ | 10 | 2.6 | 15.2 | 33.4 | 0.24 | 0.57 |
| $S_{20}$ | 20 | 1.9 | 9.6 | 23.0 | 0.25 | 0.57 |
| $S_{40}$ | 40 | 1.7 | 6.1 | 16.5 | 0.25 | 0.57 |
| $S_{60}$ | 60 | 1.3 | 4.4 | 12.7 | 0.25 | 0.58 |
| $S_{240}$ | 240 | 1.1 | 2.8 | 7.8 | 0.25 | 0.59 |

The steady shear rheology of the slurries was measured using a stress-controlled AR 1000 rheometer (TA Instruments, UK) equipped with a 40mm parallel plate geometry and roughened to eliminate wall slip. Fig. 6 shows the steady flow curves of 40 wt% slurries of different psds produced from milling for 10 – 240 min. The slurries all exhibited shear thinning behaviour. The curves lie above each other with increasing milling time showing a systematic increase in the slurry consistency as the milling time is increased (and the particle sizes are reduced). The flow curves can be fitted using the Ostwald de Waele (power law) model

$$\tau = k\dot{\gamma}^n \qquad (1)$$

where $\tau$ is the applied shear stress, $k$ is the consistency index, $\dot{\gamma}$ is the shear rate and $n$ is the power law exponent. For the $S_{60}$ slurry, values of $k = 0.25$ and $n = 0.58$ where obtained with an $R^2$ value of 0.99. Similar quality of fit was obtained for all other slurries tested. Values of $k$ and $n$ for all the slurries are given in Table 1.

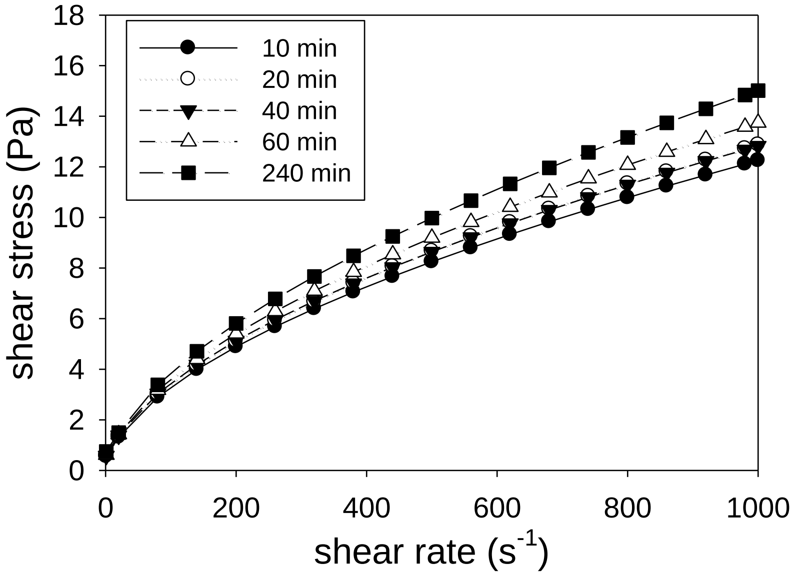

Fig. 6. Steady shear flow curves for slurries obtained at different milling times.

## 2.2. Pre-treatment and characterisation of Fecralloy foil

Commercially available Fecralloy® foil of 50 µm thickness with a composition of Fe (72.6 wt%), Cr (22.0 wt%), Al (4.80 wt%), Y (0.30 wt%) and Si (0.30 wt%) (GoodFellow, UK) was cut into coupons (50 × 80 mm). The coupons were degreased in an ultrasonic bath filled with acetone and later with distilled water. This was followed by pre-oxidation in a furnace (Lenton UK) at 950 °C for different durations of 0, 5 10 and 30 h (Wu et al., 2005; Adegbite, 2010). After pre-oxidation, the specific mass gain of the coupons as a function of pre-oxidation time was determined using a mass balance (Ohaus Corporation, USA). The two-dimensional (2D) and three-dimensional (3D) surface topographies of the Fecralloy® were measured using LPI (Talysurf CCI model, Taylor Hobson, UK). A thousand sample lengths of 5 µm each were measured, thus, covering a total evaluation length of 5 mm. From the surface topography, the following 2-D roughness parameters were obtained: the arithmetic average roughness, $R_a$ (arithmetic mean of sampled deviations from the centreline profile height), the root mean square roughness, $R_q$ (geometric mean of the sampled deviations from the centreline profile height) and the maximum peak to valley roughness, $R_t$. 3-D counterparts of these parameters are $S_a$, $S_q$ and $S_t$ respectively. Specific details of calculation of these parameters may be found in Busch *et al.* (1998).

The surface crystal composition of the coupons was determined by XRD (X' Pert Pro diffractometer, Phillips, the Netherlands) using a Fe-filtered Co Kα radiation and a power of 45 kV × 30 mA. The surface microstructure of the coupons was assessed by using a SEM-EDS (Jeol 6060 SEM, Oxford Instruments, UK).

### 2.3. Coating deposition

An automatic film applicator (Model 1132N, Sheen Instruments UK) was used to coat the slurries onto the Fecralloy coupons using a bar of nominal gap of 100 μm and a traverse speed of 100 mms$^{-1}$ (shear rate = 1000 s$^{-1}$) as shown in Fig. 7. The coated coupons were allowed to dry at room temperature, and then oven dried at 110 $^{o}$C for 1 h and finally calcined at 500 $^{o}$C for 1 h. Slurry $S_{60}$ was coated onto each pre-oxidised Fecralloy coupon in order to determine the influence of surface treatment. The full list of slurries in Table 1 was then coated onto the optimum treated surface to assess the role of particle size.

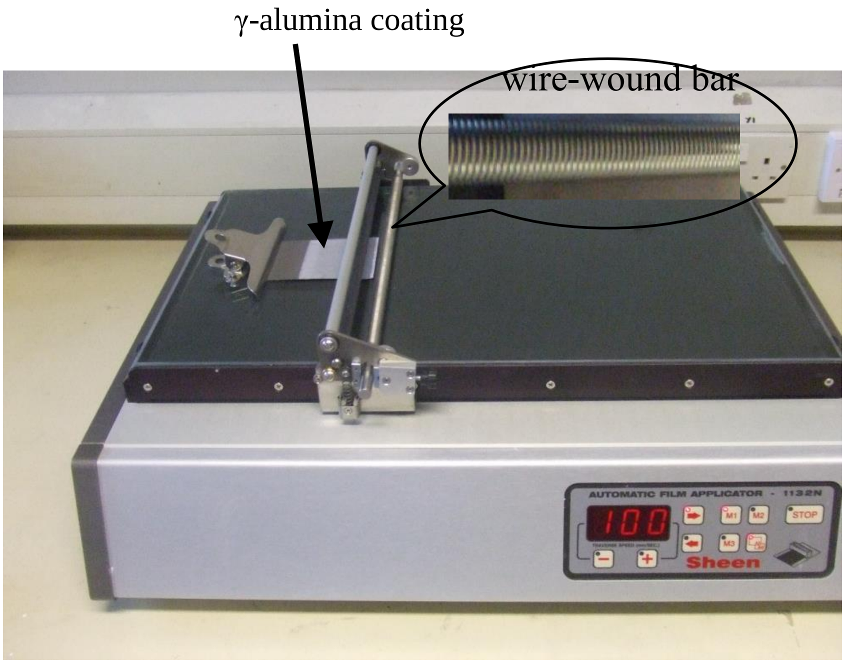

Fig. 7. An automatic film applicator showing how coating was done.

### 2.4. Coating characterisation

The coating loading of slurry on Fecralloy® surface was calculated by the percentage mass increase of the coupon after coating. The coating adhesion was determined using the ultrasonic technique and the new mechanical testing method designed to measure the failure (adhesion) strength profile of the coating.

*(a) Ultrasonic method* (e.g. Valentini *et al.*, 2001)

The coated foils were soaked into petroleum ether contained inside a sealed beaker for 30 min, then soaked in an ultrasonic water bath (300 W and 60 kHz ) for 1 h and later dried in an oven at 110°C for 2 h. The percentage mass loss was then calculated; the lower the mass loss, the better the coating adherence (Zhou *et al.*, 2007). These values were obtained by finding the average and standard deviation of 3 measurements. This was followed by a visual quality assessment of the coatings using SEM.

*(b) Mechanical testing method*

This method is comprised of a dual column mechanical testing system (MTS) (4467 series, Instron, UK) which houses a 1 kN load cell and controlled by Bluehill® software. Each coating sample produced was firmly screwed onto the platform base of the MTS using an annular support (Fig. 8(a)). A metal probe was mounted at one end to the MTS, and the other end was joined with a carbon tape (TAAB Laboratories Equipment, UK) and lowered to make contact area $A$ of $0.79 \times 10^{-4}$ $m^2$ with the coating. The programming of the probe was such that the coating was compressed at a specified load (Fig. 8(b)). The probe was then lifted up at a given withdrawal speed of 10 mm/min, which consequently resulted in the detachment of the coating from the Fecralloy® substrate. The coating remaining on the substrate is shown in Fig. 8(c), and the probe with the detached coating is shown in Fig. 8(d). The measurements taken were converted into graphs of stress versus displacement using the test profiler software which linked the MTS to a computer.

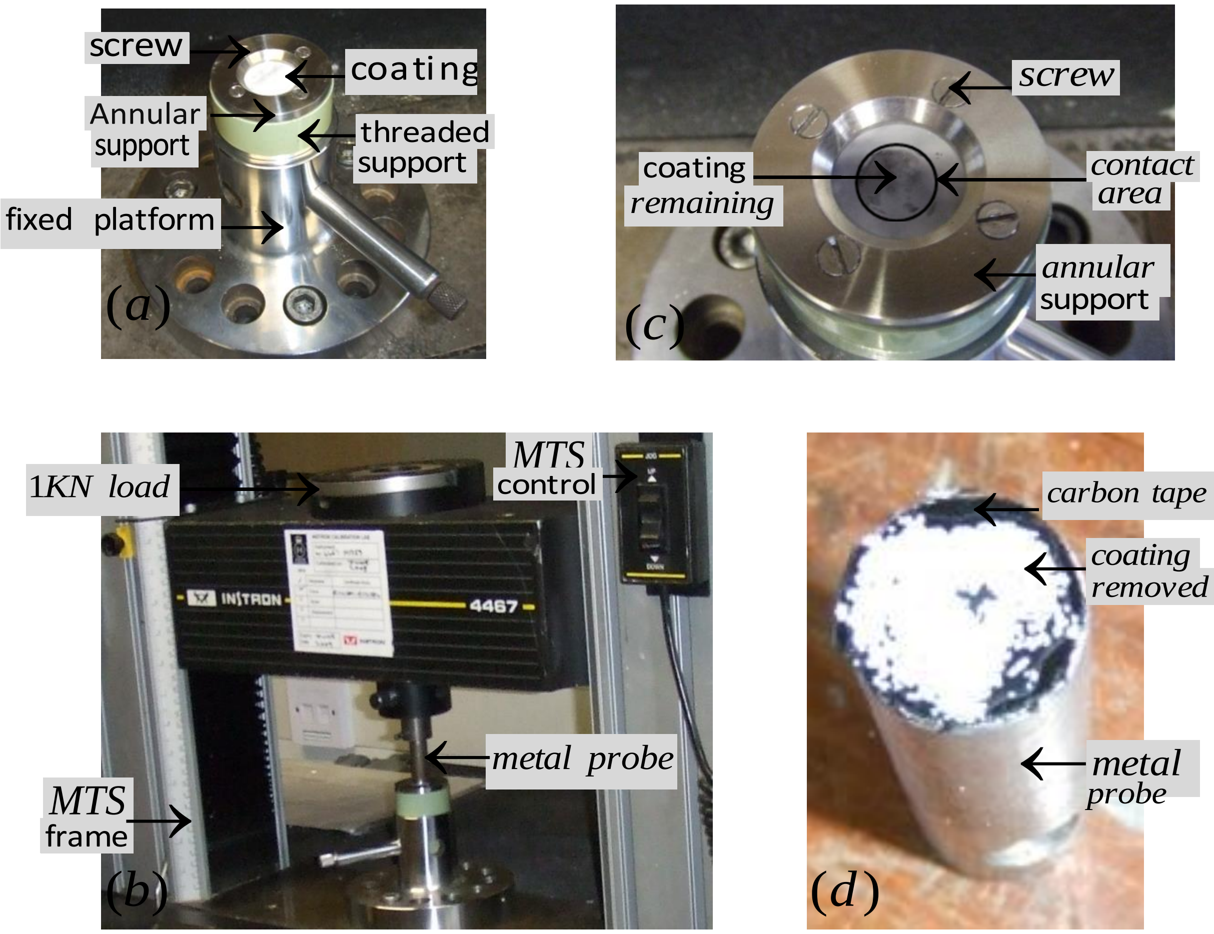

Fig. 8. Pictures showing how coating adhesion is being measured by MTS: (a) coating firmly screwed; (b) coating compressed by probe; (c) coating remaining after test and (d) probe showing coating removed.

A typical profile obtained from the MTS is represented in Fig. 9. This shows a drop in the applied compression stress as the probe was being lifted up. The point of zero is the equilibrium, i.e. the instance when no force was acting on the probe. The stress increased thereafter as the probe continued to move up, thus representing the start of tension. The moment of complete rupture (or removal) of the coating is referred to as the breaking point and the corresponding stress at this point is called the ultimate strength (Pavlina et al., 2008). The stress dropped to zero after the breaking point as the probe was finally released from tension. The ultimate strength is a very important parameter for quantifying the adhesion strength of the coating. The amount of coating removed, which is dependent on the contact area of the probe, was the mass % difference in the coatings on the substrate before and after the test.

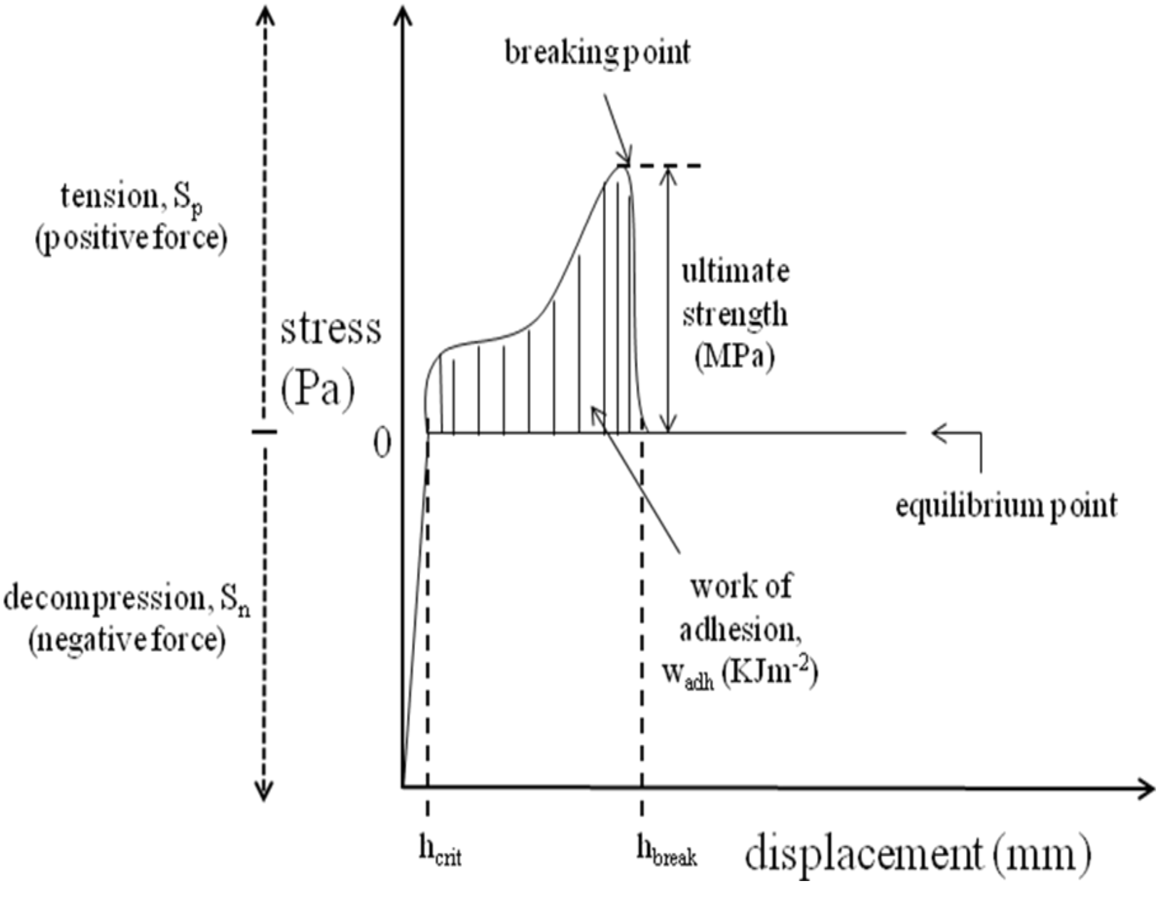

Fig. 9. MTS profile showing fundamental parameters measured.

The portion of the graph above the zero line (i.e. shaded area) is referred to as the work of adhesion, which is defined as the energy per unit area required to remove the coating from the substrate as shown in Eq. (2) (Wei and Hutchinson, 1998). This was calculated by Simpson's rule using Matlab® (The MathWorks, USA).

$$w_{adh} = \int_{h_{crit}}^{h_{break}} S_p .dh = \int_{h_{crit}}^{h_{break}} \frac{F_p}{A} .dh = \frac{1}{A} \int_{h_{crit}}^{h_{break}} F_p .dh \qquad (2)$$

where

$w_{adh}$ = work of adhesion (kJm$^{-2}$)

$S_p$ = stress on coating due to tension (MPa)

$F_p$ = force on coating due to tension (kN)

$h_{crit}$ = displacement at stabilisation stress (mm)

$h_{break}$ = displacement at breaking point (mm)

$A$ = contact area (mm$^2$)

Preliminary MTS tests were performed on coatings from slurry $S_{60}$ at different compression loads of 100, 200 and 300 N to determine the effects of compression on the coating adhesion. Subsequently, the adhesion for all the coatings were measured at a fixed compression load of 200 N using the methodology described.

## 3. RESULTS AND DISCUSSION

### 3.1. *Effect of pre-oxidation on the efficacy of Fecralloy® foil as catalyst support*

The XRD results in Fig. 10 show the surface crystal composition of the coupons pre-oxidised at 950°C for 0 – 30 h. All of the coupons had some amounts of α–alumina, Fe and Cr present on their surfaces, in line with previous findings by Badini and Laurella (2001) and Tien and Pettit (1972). The untreated surface is dominated by a Fe(Cr) peak and some small α-alumina peaks (Figure 10a).

Pre-oxidation for 5 h produced substantial amounts of θ–alumina and a small amount of α–alumina (Figure 10b). At this stage, most of the θ–alumina formed was not yet transformed into α–alumina because pre-oxidation had not sufficiently occurred. Increased pre-oxidation to 10 h produced sufficient transformation of θ-alumina into α–alumina, as the peaks of the latter are large and conspicuously visible (Fig. 10c). For these coupons, well formed α–alumina layers were predominantly present on their surface and they represented suitable compatible ingredients for coatings. Prolonged pre-oxidation for 30 h however resulted in the formation of α-alumina conglomerates as other alloy elements (i.e. Fe and Cr) were spontaneously oxidised. This is characterised by diminishing peaks of α–alumina (Fig. 10d).

The results are in accordance with the previous studies on this area (e.g. Jia et al., 2007; Nicholls and Quadakkers, 2002) which showed excellent α–alumina composition on coupon surface pre-oxidised at 950 °C for 10 h. These studies also reported that the Fecralloy® surface enrichment by aluminium during pretreatment was caused by an elemental transport process.

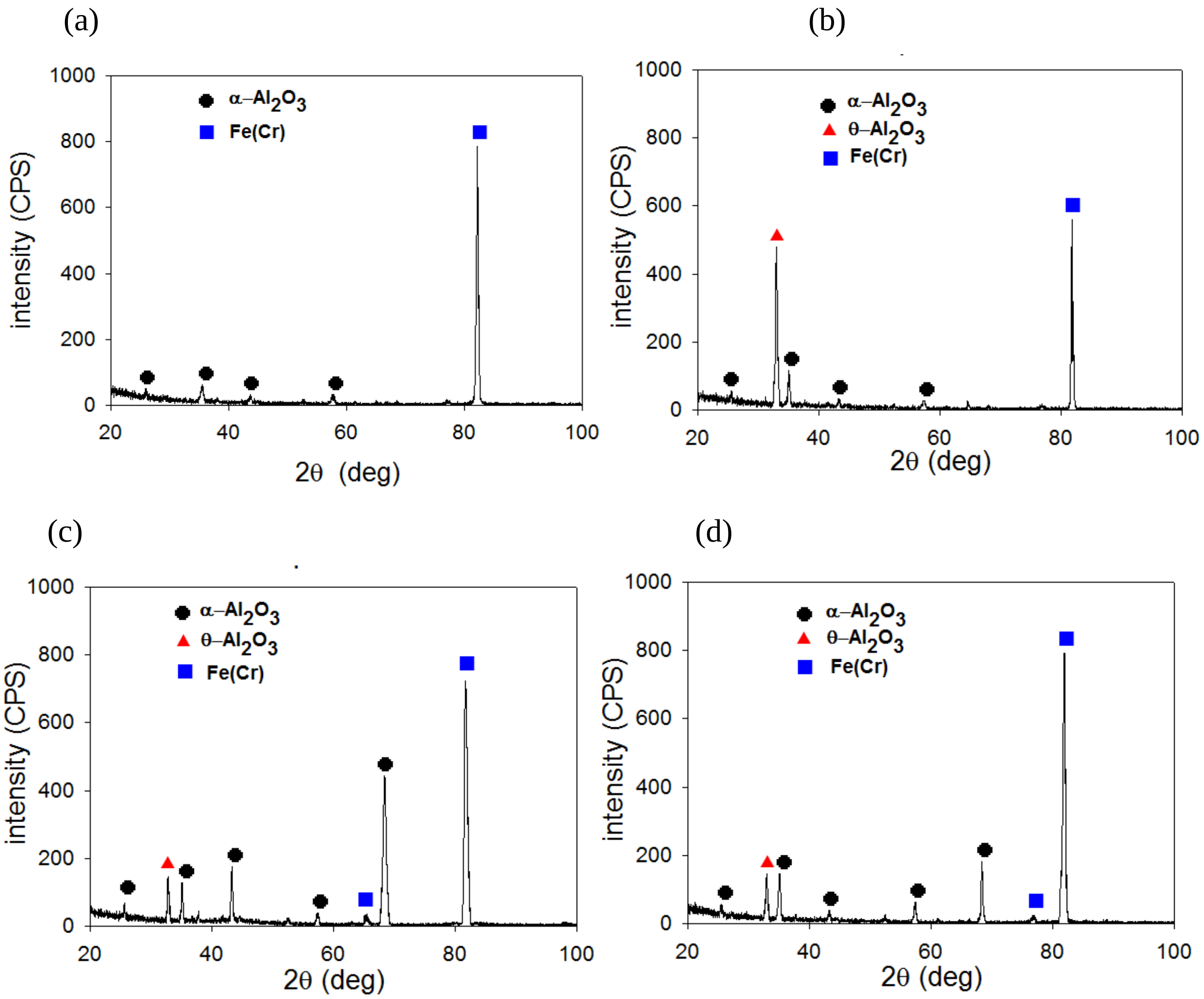
(a)
(b)
(c)
(d)

Fig. 10. XRD patterns of Fecralloy® coupons treated for (a) 0 h; (b) 5 h; (c) 10 h; (d) 30 h.

Examples of the surface topography obtained from the LPI for coupons pre-oxidised for 0 and 10 h are shown in Fig. 11. The surface of the untreated sample (Fig. 11a) is covered with surface asperities of up to ~2 µm. The asperities are not randomly oriented and linear ridges are observable: these are also present on the inset SEM image and are rolling lines formed during the manufacture of the foil. With reference to Table 2, which presents the results from the LPI, the roughness parameters for the untreated coupon are small (e.g. $R_a$ = 0.06 µm and $S_a$ = 0.20 µm). Since the surface was untransformed, the lack of surface asperities and undesirable crystal structure would be expected to cause poor coating adherence. The sample preoxidised for 10 h (Figure 11b) is much rougher, with asperities up to 10 µm given a five-fold increase over the untreated material. Again rolling lines in the sample are much more evident. The inset SEM images show that the surface is covered with randomly oriented whisker shaped structures, which from the XRD measurements are rich in α-alumina.

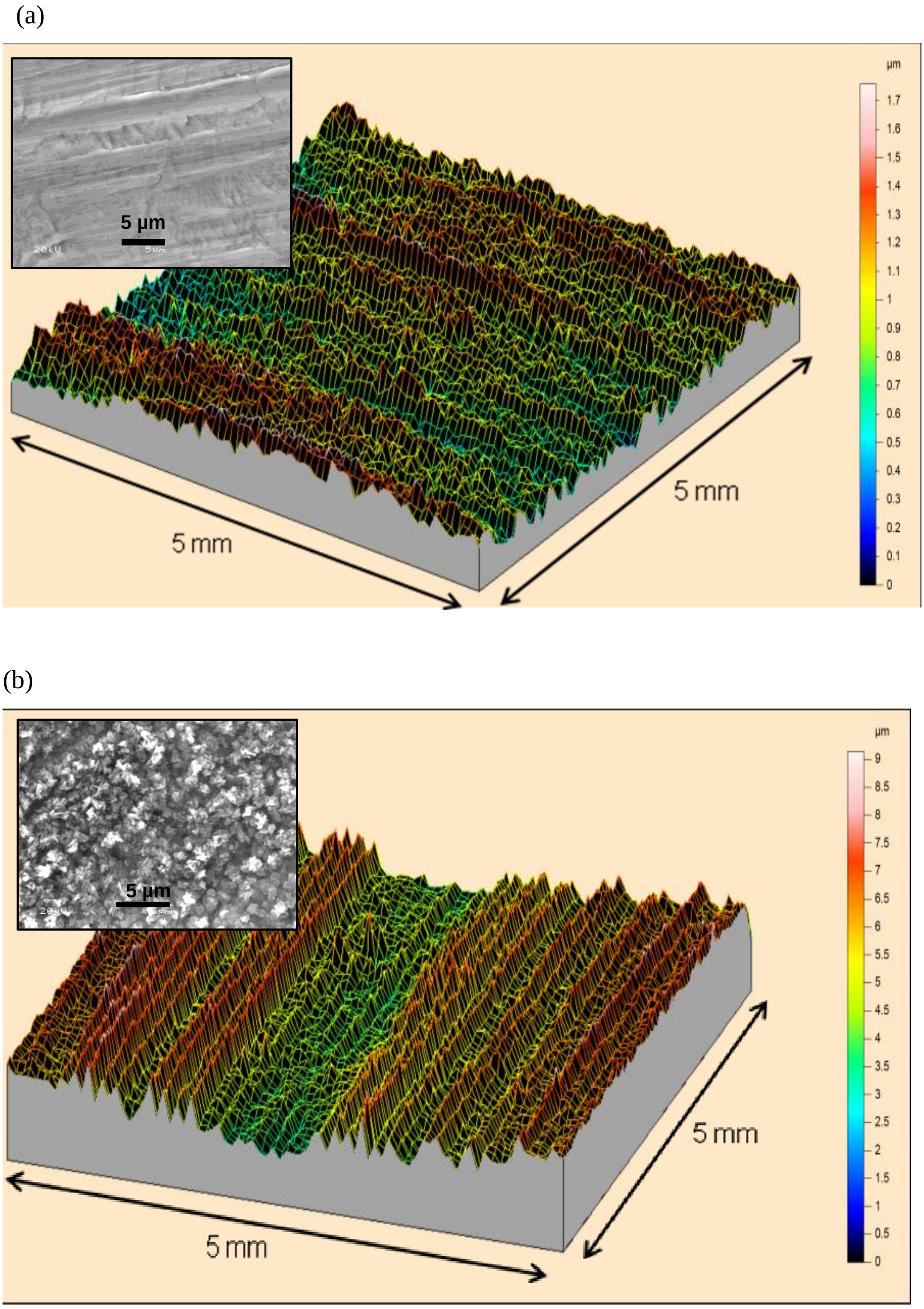

Figure 11. Topography profile and SEM image (inset) of Fecralloy® coupon treated for (a) 0 h; (b) 10 h.

Table 2 shows that the roughness of the samples increases significantly between 0 and 5 h oxidation, reaching a maximum after 10 h (e.g. $R_a$ = 0.31 μm and $S_a$ = 0.83 μm). The roughness parameters however decreased after prolonged pre-oxidation for 30 h ($R_a$ = 0.23 μm and $S_a$ = 0.52 μm), suggesting that adherent ability of the Fecralloy® may be reduced.

Table 2. Roughness parameters of Fecralloy® coupons pre-oxidised at 950 °C for 0 – 30 h obtained using LPI.

| Roughness parameters | Type | Definition | Values (µm) | | | |
|---|---|---|---|---|---|---|
| | | | 0 h | 5 h | 10 h | 30 h |
| $R_a$ | 2D | arithmetic average | 0.06 | 0.15 | 0.31 | 0.23 |
| $R_q$ | 2D | root-mean-square | 0.08 | 0.17 | 0.36 | 0.20 |
| $R_t$ | 2D | maximum peak-valley | 0.58 | 1.09 | 2.46 | 1.42 |
| $S_a$ | 3D | arithmetic average | 0.20 | 0.35 | 0.83 | 0.52 |
| $S_q$ | 3D | root-mean-square | 0.24 | 0.42 | 1.01 | 0.69 |
| $S_t$ | 3D | maximum peak-valley | 1.76 | 4.88 | 9.14 | 5.27 |

The elemental composition of the coupon surfaces obtained from EDS are given in Table 3. Initially the untreated foil surface was composed predominantly of Iron (Fe = 72.4 wt.%) and Chromium (Cr = 21.3 wt.%) with Aluminium (Al) and Oxygen (O) in much smaller amounts. After 5 h preoxidation, the amounts of Fe and Cr fell to 35.5 wt.% and 19.0 wt.% respectively whilst the Al and O both increased to 16.1 wt.% and 27.4 wt.% respectively. After 10 h pre-oxidation Al and O became the majority elements on the coupon surface at 34.6 wt.% and 37.8 wt.% respectively while the amounts of Fe and Cr both slumped (19.2 wt.% and 7.9 wt.% respectively). Prolonged pre-oxidation after 30 h resulted in a reversal of this trend with the amounts of Fe (32.5 wt.%) and Cr (13.5 wt.%) increasing at the expense of Al (25.2 wt.%) and O (26.7 wt.%). The EDS results agree with the crystal structure derived from the XRD analysis, which showed similar composition changes as a function of pre-oxidation time.

Table 3. Elemental composition of the coupon surfaces obtained from EDS.

| Element | Amounts (wt.%) | | | |
|---|---|---|---|---|
| | 0 h pre-oxidation | 5 h pre-oxidation | 10 h pre-oxidation | 30 h pre-oxidation |
| Oxygen (O) | 0.76 | 27.40 | 37.84 | 26.69 |
| Aluminium (Al) | 4.78 | 16.13 | 34.56 | 25.21 |
| Chromium (Cr) | 21.33 | 18.98 | 7.92 | 13.54 |
| Iron (Fe) | 72.47 | 36.50 | 19.19 | 32.48 |

Assessment of the adhesion of the $S_{60}$ slurry to the pre-oxidised samples using the ultrasonic adhesion test is shown in Table 4. Clearly, the duration of pre-oxidation has a major influence on the capability of the foil to perform well as a catalyst support. The slurry did not wet the surface of the untreated coupon, hence leading to virtually zero loading. The pre-oxidised coupons, however, were wetted, thereby producing coating loadings of 5.19 – 7.94

mass%. The results in Table 4 can be explained in terms of the Fecralloy® surface characterisation. For the untreated coupon, the coating loading and adhesion were unsurprisingly very poor because the foil surface was the least rough. The coupons pre-oxidised for 5 and 30 h showed improved capabilities which was commensurate with their roughness measurements in Table 2. The optimal coating loading and adhesion were obtained from the coupon with the roughest surface, i.e. the sample pre-oxidised for 10 h (Figure 12). This is because of the enhanced surface microstructure brought about by the randomly oriented α–alumina whiskers, thereby creating an ideal topography onto which coatings are firmly anchored (Jia et al. 2007). This sample was therefore used in the subsequent particle size studies.

Table 4. Coating properties for Fecralloy® coupons pre-oxidised at 950 °C for 0 – 30 h.

| Pre-oxidation time *t* (h) | 3D average roughness $S_a$ (µm) | Coating loading $M$ (mass %) | Average film thickness $f_t$ (±2µm) | Mass % loss from ultrasonic adhesion test $M_a$ |
|---|---|---|---|---|
| 0 | 0.2 | 0.08 | negligible | 99.60 |
| 5 | 0.35 | 5.19 | 27 | 19.42 |
| 10 | 0.83 | 7.94 | 38 | 9.89 |
| 30 | 0.52 | 6.75 | 33 | 16.30 |

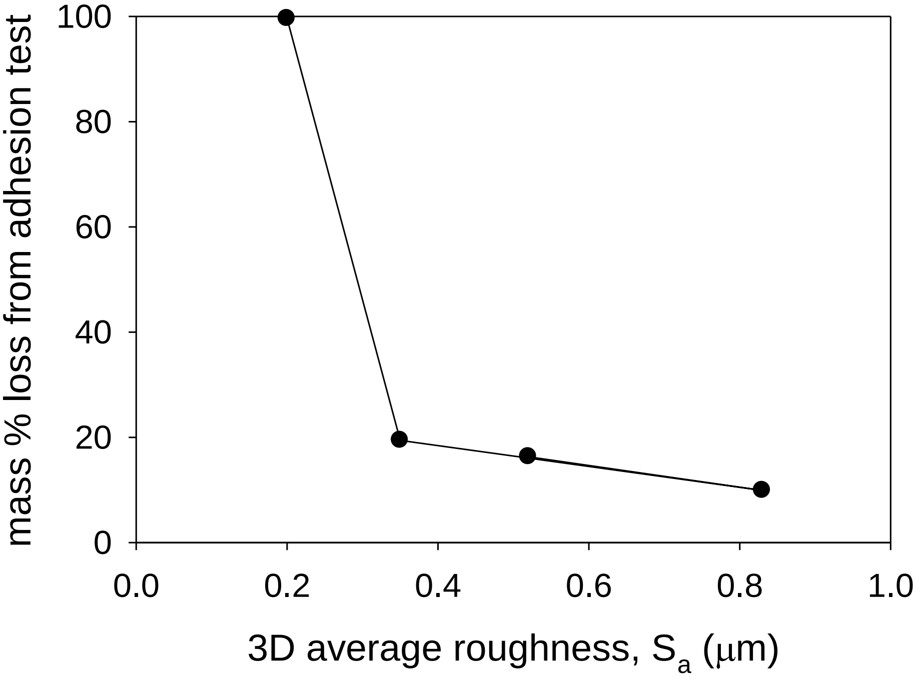

Fig.12. Mass % loss from adhesion test for Fecralloy coupons coated with $S_{60}$ slurry versus Fecralloy® 3D average roughness, $S_a$.

### *3.2. Effect of slurry particle size on coating adhesion.*

SEM images of coatings produced from slurries $S_{10}$ – $S_{240}$ are shown in Fig. 13. The images show that the thickness of the coating decreases with deceasing particle size (increased milling time) and that the particles also become more tightly packed. Cracks are evident within the coating structure for the $S_{10}$ slurry in Figure 13a, but it is not possible to discern whether this is an artefact of the preparation process for SEM.

Coating properties for the slurries are presented in Table 5, together with data from the ultrasonic adhesion test. Coating loadings are reasonably constant for all slurries (7-8 mass %), yet the coating thicknesses obtained from the SEM images show a decrease of 30% from the slurry with the largest particles ($S_{10}$) to the smallest ($S_{240}$). Therefore the voids between the particles within the coating must decrease by a corresponding amount. Mass loss from ultrasonic test is very high (37.3%) for the $S_{10}$ slurry, and falls rapidly to < 10% as the $d_{0.9}$ falls to less than 12-13 µm. Notably, these particle sizes are of comparable size to the asperities of roughness of the Fecralloy® surface ($S_t$ = 9.14 µm, see Table 2), suggesting that mechanical interlocking between the particles and the surface plays a part in the adhesion mechanism.

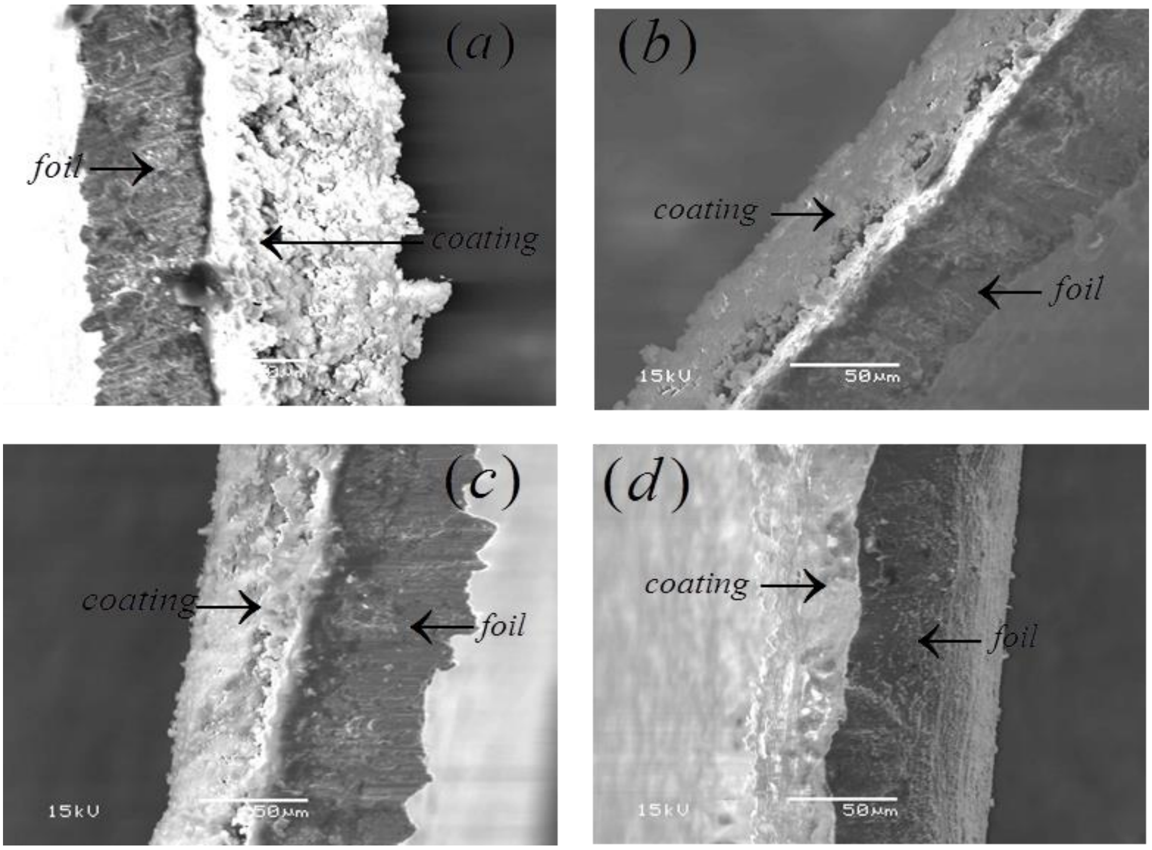

Fig. 13 SEM images of Fecralloy coatings of different particle size distributions $d_{0.9}$ of (a) 33.4 µm; (b) 16.5 µm; (c) 12.7 µm and (d) 7.8 µm.

Table 5. Coating adhesion properties using ultrasonic test for $S_{10} – S_{240}$.

| Slurry | 90% diameter $d_{0.9}$ (µm) | Coating loading $M$ (mass %) | Average film thickness $f_t$ (±2 µm) | Mass % loss from ultasonic adhesion test $M_a$ |
|---|---|---|---|---|
| $S_{10}$ | 33.42 | 7.4 | 53 | 37.3 |
| $S_{20}$ | 23.02 | 7.5 | 44 | 28.0 |
| $S_{40}$ | 16.47 | 8.1 | 40 | 15.5 |
| $S_{60}$ | 12.74 | 8.0 | 38 | 9.9 |
| $S_{240}$ | 7.82 | 7.8 | 37 | 8.0 |

### *3.3. Comparison of mechanical testing system (MTS) and ultrasonic adhesion measurements.*

The coatings used in these tests were produced from slurries $S_{S10}$, $S_{S40}$ and $S_{S60}$. Fig. 14 shows the MTS profiles of the stress as a function of displacement for all the coatings assessed. All the three plots have similar profiles: decompression until the stress was zero at equilibrium, followed by increased stress at tension until the ultimate strength was attained at coating removal, and finally the attainment of equilibrium. It is shown that the ultimate strength – which is the determinant of the adhesion quality – is dependent on the particle diameter of coatings. The highest ultimate stress of 0.59 MPa, inferring best adhesion, was achieved by the coatings from slurry $S_{S60}$ ($d_{0.9}$ of 12.74 µm), followed by 0.29 MPa for $S_{S40}$ ($d_{0.9}$ of 16.47 µm), and then the least ultimate strength of 0.10 MPa from $S_{S10}$ ($d_{0.9}$ of 33.42 µm). Similarly, the ultimate strength and the work of adhesion both followed the same trend as they all increased with finer coating particles. Furthermore, the coating amounts removed were influenced by the particle diameter $d_{0.9}$ as presented in the detailed results shown in Table 6.

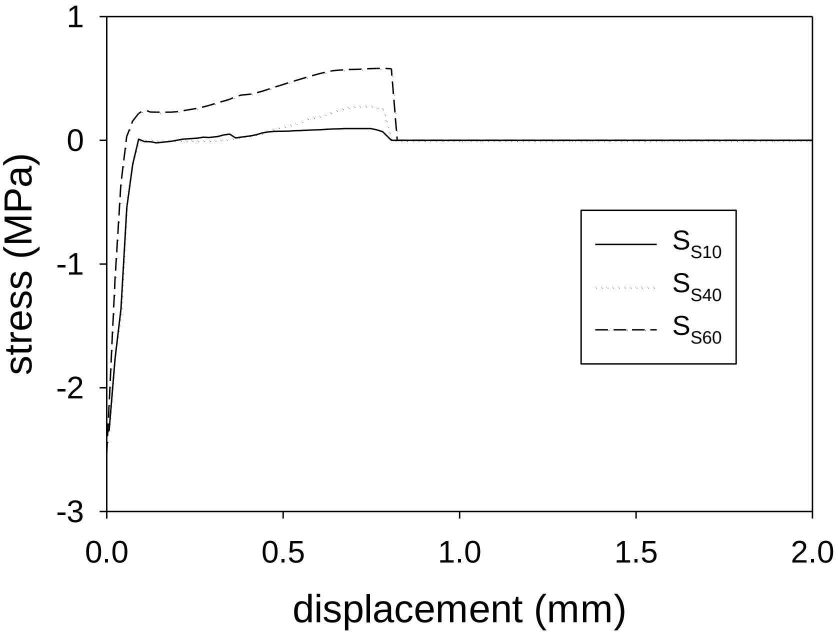

Fig. 14. MTS profiles for coatings from slurries $S_{S10}$, $S_{S40}$ and $S_{S60}$.

Table 6. MTS results for coatings from slurries $S_{10}$, $S_{40}$ and $S_{60}$.

| Slurry type | Diameter $d_{0.9}$ (µm) | Ultimate strength (MPa) | Amount removed (mass % contact area) | Work of adhesion ($kJm^{-2}$) |
|---|---|---|---|---|
| $S_{10}$ | 33.42 | 0.10 | > 97 | 0.03 |
| $S_{40}$ | 16.47 | 0.29 | 88 – 93 | 0.07 |
| $S_{60}$ | 12.74 | 0.59 | 85 – 90 | 0.33 |

In addition to requiring the lowest ultimate strength of 0.10 MPa, the coatings from large particles were almost totally removed (more than 97 mass %) from the contact surface area. The finest coatings, on the other hand, had the least removal (85 – 90 mass %) at the highest ultimate strength of 0.59 MPa (see coating pictures in Fig. 15). These behaviours confirm cohesive failure (i.e. internal coating fractures) for fine particles rather than adhesive failure (i.e. coating peeling off the surface) exhibited by large particles.

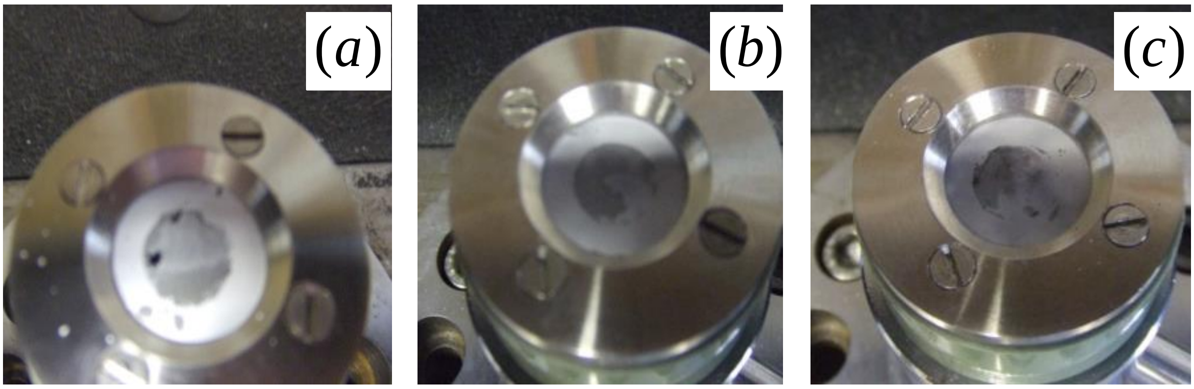

Fig. 15. Coating pictures after MTS tests showing amounts removed: (a) $S_{10}$; (b) $S_{40}$ and (c) $S_{60}$.

The measurements by ultrasonic vibration given in Table 7 also show the same pattern, i.e. low mass % coating loss by finer particles. For finer particles of $d_{0.9}$ not exceeding 12.74 µm, the coating loss from ultrasonic vibration was less than 10 mass % coating loss. This is because finer particles, unlike their large counterparts, properly penetrated and anchored onto the rough asperities on the Fecralloy® surface, therefore leading to good coating adhesion. It is therefore established from all the results that finer particles had better coating adhesion.

Table 7. Ultrasonic vibration results for coatings from slurries $S_{10} - S_{240}$.

| Slurry type | $d_{0.9}$ (µm) | Coating loading (mass %)<br>SD = ± 2.5 % of loading | Average film thickness<br>(± 2 µm) | Mass % loss from ultrasonic adhesion test<br>SD = ± 3.3 % of loss |
|---|---|---|---|---|
| $S_{10}$ | 33.42 | 7.4 | 53 | 37.3 |
| $S_{20}$ | 23.02 | 7.5 | 44 | 28.0 |
| $S_{40}$ | 16.47 | 8.1 | 40 | 15.5 |
| $S_{60}$ | 12.74 | 8.0 | 38 | 9.9 |
| $S_{240}$ | 7.82 | 7.8 | 37 | 8.0 |

## 4. CONCLUDING REMARKS

A detailed study of the influence of Fecralloy pre-oxidation and particle size on γ-alumina coating adhesion has been undertaken. The XRD measurements have shown optimal amounts of α-alumina crystals on the Fecralloy® surface after 10 h heat treatment at 950°C, and this condition also corresponds with the maximum surface roughness observed using LPI. The SEM micrographs show that the Fecralloy coupon pre-oxidised at 950 °C for 10 h was characterised by uniform, conspicuous and randomly oriented α-alumina whiskers which promote good coating adhesion.

Slurries with different particle sizes were obtained by milling a 40 wt.% aqueous mixture of γ-alumina particles at a pH value of 4 using acetic acid. The slurries all showed shear-thinning behaviour. Steady state flow behaviours obtained after 25 s of pre-shear were adequately described by the Ostwald de Waele constitutive law.

The coating deposition the γ-alumina slurries onto the pre-oxidised Fecralloy® surface was achieved using an automatic film applicator at a controlled shear rate, enabling reproducible coating thicknesses to be obtained. The best coating adhesion was found for the slurries with a $d_{0.9} < 12$ µm, which lost less than 10% of their mass during an ultrasonic adhesion test. Notably, these particles sizes are of similar magnitude to the asperities on the pre-oxidised surface suggesting that mechanical interlocking plays an important role in providing good surface adhesion.

A new adhesion method, based on use of a mechanical testing system (MTS), enabled the strength of the coatings to be assessed in terms of the ultimate stress at coating failure and work of adhesion. Of the three coatings tested, the $S_{60}$ slurry coating had the greatest ultimate stress of 0.59 MPa, six times the value for the $S_{10}$ slurry. The work of adhesion was an order of magnitude higher. These results suggest that the new MTS method has potential as a means of obtaining fundamental mechanical properties of the coatings, rather than the empirical nature of existing adhesion tests.

## ACKNOWLEDGEMENTS

The author gratefully acknowledges the funding by the EPSRC and Johnson Matthey Plc. The views expressed in this article are those of the author and do not necessarily reflect the views of the sponsors.

## REFERENCES

1) Adegbite, SA. Coating of catalyst supports: links between slurry characteristics, coating process and final coating quality, University of Birmingham, PhD thesis, 2010, pp. 113-229.
2) Acres, GJK, and Harrison, B. The development of catalysts for emission control from motor vehicles: early research at Johnson Matthey, Topics in Catalysis, 2004, 28 (1-4), pp. 3-11.
3) Agrafiotis, C, Tsetsekou, A and Leon, I. Effect of slurry rheological properties on the coating of ceramic honeycombs with yttria-stabilized-zirconia washcoats, Journal of the American Ceramic Society, 2000, 83 (5), pp. 1033-1038.
4) Avila, P, Montes, M and Miro, EE. Monolithic reactors for environmental applications - a review on preparation technologies, Chemical Engineering Journal, 2005, 109 (1-3), pp. 11-36.
5) Badini, C and Laurella, F. Oxidation of FeCrAl alloy: influence of temperature and atmosphere on scale growth rate and mechanism, Surface & Coatings Technology, 2001, 135 (2-3), pp. 291-298.
6) Barnes, HA. Measuring the viscosity of large-particle (and flocculated) suspensions - a note on the necessary gap size of rotational viscometers, Journal of Non-Newtonian Fluid Mechanics, 2000, 94 (2-3), pp. 213-217.
7) Burgos, N, Paulis, MA and Montes, M. Preparation of $Al_2O_3$/Al monoliths by anodisation of aluminium as structured catalytic supports, Journal of Materials Chemistry, 2003, 13 (6), pp. 1458-1467.
8) Busch, T, Harlow, R and Thompson, RL. Surface measurements. In: Fundamentals of dimensional metrology. 3rd edn, Delmar Publishers, New York, 1998, pp. 499-524.
9) Collins, NR and Twigg, MV. Three-way catalyst emissions control technologies for spark-ignition engines - recent trends and future developments, Topics in Catalysis, 2007, 42-43, pp. 323-332.
10) Cybulski, A and Moulijn, JA, Structured catalysis and reactors, 2nd edn, Taylor & Francis, London, 2006.
11) Cybulski, A and Moulijn, JA. Modelling of heat transfer in metallic monoliths consisting on sinusoidal cells, Chemical Engineering Science, 1994, 49 (1), pp. 19-27.
12) Fei, W, Kuiry, SC, Sohn, Y and Seal, S. Sol gel alumina coating on Fe-Cr-Al-Y fibre media for catalytic converters, Surface Engineering, 2003, 19 (3), pp. 189-194.
13) Germani, G, Stefanescu, A, Schuurman, Y and van Veen, AC. Preparation and characterization of porous alumina-based catalyst coatings in microchannels, Chemical Engineering Science, 2007, 62 (18-20), pp. 5084-5091.
14) Haagen-Smit, AJ, Bradley, CE, and Fox, MM. Industrial & Engineering Chemistry Research, 1953, 45, 2086.
15) Housecroft, CE and Constable, EC. An introduction to organic, inorganic and physical chemistry, 2nd edn, Pearson Education Limited, Essex, 2002.

16) Janickle, MT, Kestenbaum, H, Hagendorf, U, Schuth, F, Fichtner, M and Schubet, K. The controlled oxidation of hydrogen from an explosive mixture of gases using a microstructured reactor/heat exchanger and Pt/$Al_2O_3$ catalyst, Journal of Catalysis, 2000, 191 (2), pp. 282-293.

17) Jia, LW, Shen, MQ and Wang, J. Preparation and characterization of dip-coated γ-alumina based ceramic materials on FeCrAl foils, Surface & Coatings Technology, 2007, 201 (16-17), pp. 7159-7165.

18) Jobson, E. Future challenges in automotive emmision control, Topics in Catalysis, 2004, 28 (1-4), pp. 191-199.

19) Kestenbaum, H, de Oliveira, AL, Schmidt, W, Schuth, F, Ehrfeld, W, Gebauer, K, Lowe, H, Richter, T, Lebiedz, D, Untiedt, I and Zuchner, H. Silver-catalysed oxidation of ethylene to ethylene oxide in a microreaction system, Industrial & Engineering Chemistry Research, 2002, 41 (4), pp. 710-719.

20) Meille, V, Pallier, S, Bustamante, G, Roumanie, M, and Reymond, J. Deposition of γ-$Al_2O_3$ layers on structured supports for the design of new catalytic reactors, Applied Catalysis A-General, 2005, 286, pp. 232-238.

21) Nicholls, JR and Quadakkers, WJ. Materials issues relevant to the development of future metal foil automotive catalytic converters. In: Bode, H. (ed) Materials aspects in automotive catalytic converters. Wiley-VCH, Weinheim, 2002, p. 31.

22) Nievergeld, AJ. Automotive exhaust gas conversion: reaction kinetics, reactor modeling and control, PhD thesis, 1998, University of Technology, Eindhoven.

23) Pavlina, EJ and Van Tyne, CJ. Correlation of yield strength and tensile strength with hardness of steel, Journal of Materials Engineering and Performance, 2008, 17 (6), pp. 888-893.

24) Roth, T, Kloos, K, and Broszeit, E. Structure, internal stresses, adhesion and wear resistance of sputtered alumina coatings, Thin Solid Films, 1987, 153, pp. 123-133.

25) Sha, W, Xu, X, Keong, KG, Electroless copper and nickel-phosphorus plating: processing, characterisation and modelling, Woodhead Publishing, Cambridge, 2011, p. 35

26) Sun, H, Quan, X., Chen, S, Zhao, HM and Zhao, YZ. Preparation of well-adhered γ-$Al_2O_3$ washcoat on metallic wire mesh monoliths by electrophoretic deposition, Applied Surface Science, 2007, 253 (6), pp. 3303-3310.

27) Tien, JK and Pettit, FS, Mechanism of oxide adherence on Fe-25Cr-4Al (y Or Sc) alloys. Metallurgical Transactions, 1972, 3 (6), p. 1587.

28) Truyen, D, Courty, M, Alphonse, P and Ansart, F, Catalytic coatings on stainless steel prepared by sol-gel route. Thin Solid Films, 2006, 495, pp. 257-261.

29) Twigg, MV, Progress and future challenges in controlling automotive exhaust gas emissions. Applied Catalysis B-Environmental, 2007, 70 (1-4), pp. 2-15.

30) Twigg, MV, Roles of catalytic oxidation in control of vehicle exhaust emissions. Catalysis Today, 2006, 117(4), pp. 407-418.

31) Valentini, M, Cristiani, G, Levi, M, Tronconi, E and Forzatti, P. The deposition of γ-$Al_2O_3$ layers on ceramic and metallic supports for the preparation of structured catalysts, Catalysis Today, 2001, 69 (1-4), pp. 307-314.

32) Wei, Y and Hutchinson, JW. Interface strength, work of adhesion and plasticity in the peel test, International Journal of Fracture, 1998, 93, pp. 315-333.
33) Williams, JL, Monolith structures, materials, properties and uses. Catalysis Today, 2001, 69 (1-4), pp. 3-9.
34) Wu, XD, Weng, D, Zhao, S, and Chen, W. Influence of an aluminized intermediate layer on the adhesion of a $\gamma$-$Al_2O_3$ washcoat on FeCrAl, Surface & Coatings Technology, 2005, 190 (2-3), pp. 434-439.
35) Zhao, S, Zhang, JZ, Weng, D and Wu, XD. A method to form well-adhered $\gamma$-$Al_2O_3$ layers on FeCrAl metallic supports, Surface & Coatings Technology, 2003, 167 (1), pp. 97-105.
36) Zhou, J, Jia, JS, Zhang, HU, Yuan, ZS and Wang, SD. The influence of preparative parameters on the adhesion of alumina washcoats deposited on metallic supports, Applied Surface Science, 2007, 253 (23), pp. 9099-9104.